RadioGraphics

US of the Shoulder: Non–Rotator Cuff Disorders[1]

Carlo Martinoli, MD • Stefano Bianchi, MD • Nicolò Prato, MD
Francesca Pugliese, MD • Maria Pia Zamorani, MD • Maura Valle, MD
Lorenzo E. Derchi, MD

CME FEATURE

See accompanying test at http://www.rsna.org/education/rg_cme.html

LEARNING OBJECTIVES FOR TEST 3

After reading this article and taking the test, the reader will be able to:

- Identify the main US findings in non–rotator cuff abnormalities of the shoulder.
- Describe the proper technique for imaging non–rotator cuff disorders.
- Discuss the utility of US in evaluating these pathologic conditions.

SUPPLEMENTAL MATERIAL

Movie clips to supplement this article are available online at radiographics.rsnajnls.org/cgi/content/full/23/2/381/DC1.

The most common indication for shoulder ultrasonography (US) is the diagnosis of rotator cuff disease. However, there is a spectrum of non–rotator cuff abnormalities that are amenable to US examination, including instability of the biceps tendon, glenohumeral joint, and acromioclavicular joint; arthropathies and bursites (inflammatory diseases, degenerative and infiltrative disorders, infections); nerve entrapment syndromes; and space-occupying lesions. Many of these conditions may be overlooked clinically or can even mimic rotator cuff tears, and US can help redirect the diagnosis if a complete shoulder examination rather than a simple rotator cuff assessment is performed. In addition, US can be remarkably helpful in guiding either needle aspiration procedures or local injection therapy in patients with synovial processes. Although radiography, magnetic resonance (MR) imaging, and computed tomographic and MR arthrography are effective modalities for the evaluation of non–rotator cuff disorders, US is both less costly and less invasive and will likely be used more frequently in this setting as experience increases. Once adequate radiographs have been obtained to exclude apparent bone disorders, high-resolution US should be the first-line imaging modality in the assessment of non–rotator cuff disorders of the shoulder, assuming the study is performed with high-end equipment by an experienced examiner.

Abbreviations: ACJ = acromioclavicular joint, CHL = coracohumeral ligament, GHJ = glenohumeral joint, GRE = gradient-recalled-echo, LBT = long head of the biceps tendon, SA-SD = subacromial-subdeltoid, THL = transverse humeral ligament

Index terms: Shoulder, anatomy, 41.92 • Shoulder, arthritis, 41.71, 41.772 • Shoulder, dislocation, 41.42 • Shoulder, injuries, 41.481 • Shoulder, US, 41.1298

RadioGraphics 2003; 23:381–401 • **Published online** 10.1148/rg.232025100

[1]From the Cattedra "R" di Radiologia-DICMI, Università di Genova, Largo Rosanna Benzi 8, 16132 Genoa, Italy (C.M., F.P., L.E.D.); the Department of Radiology, Hôpital Cantonal Universitaire, Geneva, Switzerland (S.B., M.P.Z.); the Department of Radiology, Ospedale San Carlo, Genoa, Italy (N.P.); and the Department of Radiology, Istituto Giannina Gaslini, Genoa, Italy (M.V.). Recipient of a Cum Laude award for an education exhibit at the 2001 RSNA scientific assembly. Received May 20, 2002; revision requested June 13 and received July 26; accepted August 1. **Address correspondence to** C.M. (e-mail: *martinoli@zeus.newnetworks.it*).

Introduction

The shoulder is one of the anatomic areas that is most commonly evaluated with musculoskeletal ultrasonography (US). When performed with appropriate equipment by skilled operators, US is widely recognized as a means of accurately assessing rotator cuff disease, with a sensitivity and specificity as high as 90%–95% in the assessment of both partial- and full-thickness tears (1,2). Nevertheless, radiologists as a whole are poorly informed regarding the contributions that US can make in the assessment of non–rotator cuff abnormalities such as instability problems, synovial joint diseases, and nerve entrapment syndromes. Only a few US studies have been conducted to evaluate these conditions, and most of these studies describe only a limited number of cases or lack a standard of reference. Thus, US probably remains underused in this context. Other imaging modalities such as magnetic resonance (MR) imaging and computed tomographic (CT) and MR arthrography will probably remain the modalities of choice for diagnosing most non–rotator cuff disorders: With these modalities, image acquisition is less operator dependent and evaluation of anatomic relationships and soft-tissue structures (eg, capsule, labrum, bone) is intuitively easier and can be more readily performed. However, high-resolution US is quick, noninvasive, and inexpensive and has specific advantages over MR imaging. These advantages, which include the capacity for higher resolution and for examining tissues in both static and dynamic states with the patient in different positions, warrant the wider use of US in the evaluation of non–rotator cuff disorders.

In this article, we review the major types of non–rotator cuff abnormalities that can be diagnosed with US, with emphasis on musculoskeletal anatomy, US technique, and main US findings. Because of the wide range and heterogeneity of these abnormalities, we arbitrarily grouped them into instability problems, arthropathies and bursites, nerve entrapment syndromes, and space-occupying lesions.

Instability Problems

Because of its wide range of motion, the shoulder is susceptible to dislocations, subluxations, and lesions related to chronic stress in the surrounding soft tissues. Regardless of the type of abnormality or instability pattern, a combination of different osseous and soft-tissue restraints such as the ligaments, tendons, labrum, and capsule have increasingly received recognition either as stabilizers or as structures that sustain secondary damage in these situations. The main shoulder structures that can be evaluated with US in patients with instability problems are the long head of the biceps tendon (LBT), the glenohumeral joint (GHJ), and the acromioclavicular joint (ACJ).

Biceps Tendon

Because of its curvilinear course and its reflection over the humeral head, the LBT is prone to medial displacement, especially during powerful contraction of the biceps muscle or maximal external rotation. The tendon is retained in its proper anatomic location by the conformation of the humeral biceps sulcus and by various tendinous and ligamentous structures encountered at three different levels along its course. From cranial to caudal, these structures are the coracohumeral ligament (CHL) and superior glenohumeral ligament, the transverse humeral ligament (THL), and the tendon of the pectoralis major muscle.

The LBT enters the GHJ through the rotator cuff interval, the space between the subscapularis and supraspinatus tendons. The rotator cuff interval also houses the CHL, which courses above the LBT and then bifurcates, blending with the adjacent cuff tendons and the underlying joint capsule (Fig 1a). The anterior band of the CHL joins with the superior glenohumeral ligament to form a strong sling, commonly referred to as the reflection pulley, which inserts into the lesser tuberosity and stabilizes the LBT before the LBT enters the bicipital groove, thus protecting it against anterior shearing stress (3–5). High-resolution US can depict the CHL. Proper positioning is achieved when the patient extends the lower arm posteriorly by placing the palm of the hand on the superior aspect of the iliac wing with the elbow flexed and directed toward midline. This position causes maximal opening of the rotator cuff interval. The intraarticular portion of the LBT flattens as it is stretched against the humeral cartilage, and the CHL is tightened between the

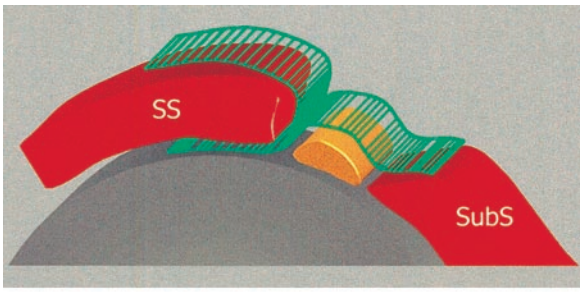

a.

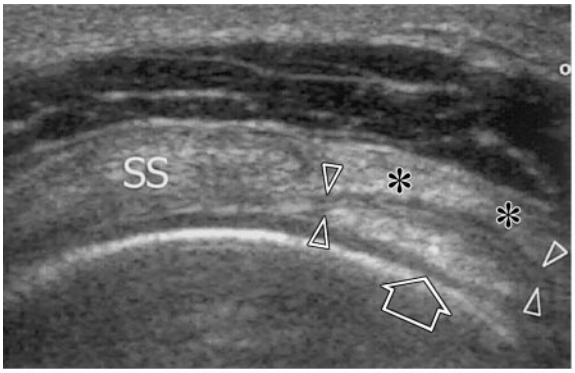

b.

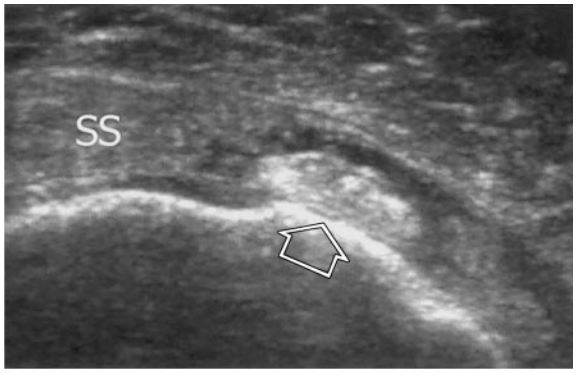

c.

Figure 1. Rotator cuff interval. **(a)** Schematic illustrates the relationship of the CHL (green) to the subscapularis (*SubS*) and supraspinatus (*SS*) tendons. The ligament forms the roof of the intraarticular portion of the biceps tendon (orange). **(b)** Corresponding transverse 12–5-MHz US image demonstrates the flattened, echogenic intraarticular portion of the biceps tendon (arrow) anterior to the supraspinatus tendon (*SS*). The CHL (*) is seen as an echogenic band of tissue superficial to the biceps tendon. A thin hypoechoic layer (arrowheads) bulges from the deep edge of the supraspinatus tendon and intervenes between the ligament and the biceps tendon, a finding that may represent the capsular interface. **(c)** Transverse 12–5-MHz US image obtained in a 42-year-old man with a surgically confirmed lesion in the rotator cuff interval that involved the CHL and the fibers of the superior capsule shows hypoechoic fluid surrounding an intact biceps tendon (arrow). Note the absence of the CHL. *SS* = supraspinatus tendon.

subscapularis and supraspinatus tendons. The CHL appears as a thick, homogeneously echogenic band of tissue that covers the LBT; it measures 2–3 mm in thickness and can be differentiated from the LBT because it is less anisotropic (Fig 1b). Its deep margin is delineated by a thin hypoechoic layer that bulges anteriorly from the deep edge of the supraspinatus tendon, possibly representing an interface between this ligament and the joint capsule. Although US cannot help detect the superior glenohumeral ligament, depiction of a normal-appearing CHL with absence of intraarticular fluid around the LBT almost always indicates an intact rotator cuff interval. When the CHL is torn, the intraarticular portion of the LBT may appear surrounded by fluid (possibly on both sides) and elevated from the humeral cartilage (Fig 1c). In such cases, the LBT may exhibit increased mediolateral motion during rotational movements (see Movie 1 at *radiographics.rsnajnls.org/cgi/content/full/23/2/381/DC1*). Chronic microtraumas can lead to early degeneration of the LBT and fissures in the inferior aspect of the tendon. Disruption of the superior border of the subscapularis tendon is almost invariably associated with these lesions (6).

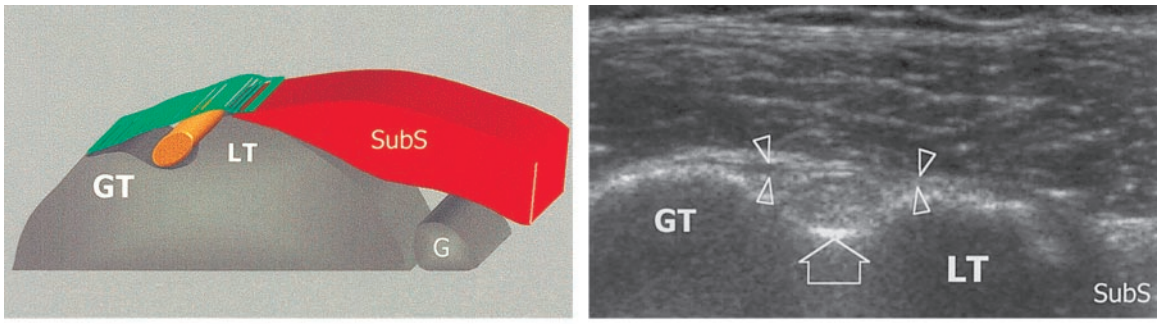

a. b.

Figure 2. Biceps tendon groove. **(a)** Schematic illustrates how the biceps tendon (orange) is located between the greater tuberosity (*GT*) and the lesser tuberosity (*LT*) and covered by the THL (green). *G* = glenoid region of the scapula, *SubS* = subscapularis tendon. **(b)** Corresponding transverse 12–5-MHz US image demonstrates the THL (arrowheads) as a thin echogenic layer that overlies the biceps tendon (arrow). The bone groove has a normal size and shape. *GT* = greater tuberosity, *LT* = lesser tuberosity, *SubS* = subscapularis tendon.

The THL is in distal continuity with the CHL and is composed of the most superficial fibers of the subscapularis tendon. The THL bridges the lesser and greater tuberosities, thereby transforming the bicipital sulcus into an osteofibrous tunnel (Fig 2a). However, the THL is weak, and its role in stabilizing the LBT just distal to its exit from the rotator cuff interval is not considered important unless the CHL is torn (5,6). Careful scanning with the transducer placed in a transverse position over the tuberosities is required to recognize the instability of the LBT at the humeral groove. The normal THL can be seen as a thin echogenic layer that overlies the bicipital sulcus (Fig 2b). In the proximal groove, an LBT that rests against the medial wall of the sulcus is a normal finding. The tendon is referred to as subluxated when it is perched over the tip of the lesser tuberosity and as dislocated when it lies on the outer slope of the groove (7,8). The LBT does not undergo medial subluxation or dislocation out of the bicipital groove when the CHL is intact, even with subscapularis tendon tear (6). On the other hand, if the CHL is torn but the subscapularis tendon is intact, the LBT can become dislocated superficial to the tendon (Fig 3a, 3b; see also Movie 2 at *radiographics.rsnajnls.org/cgi/content/full/23/2/381/DC1*) (5,6). The most common condition, however, is tearing of both the subscapularis tendon and the CHL (Fig 3c, 3d). In such cases, the disruption of the subscapularis tendon may allow the LBT to slip medially over the lesser tuberosity within the GHJ (see Movie 3 at *radiographics.rsnajnls.org/cgi/content/full/23/2/381/DC1*). Scanning with the patient's arm in external rotation can accentuate the subluxation of the LBT and further increase sensitivity to this condition. In acute dislocation, the US diagnosis is based on the absence of the LBT within the groove and its detection in a more medial position (8). Occasionally, the dislocated LBT may be difficult to identify due to its location deep within the GHJ. Transverse imaging at a more distal level can allow visualization of the LBT surrounded by a hypoechoic effusion; then, the tendon can be followed upward to its intraarticular portion. Difficulties may also arise in long-standing dislocations, in which the empty groove may be filled with echogenic fibrous scar tissue that mimics a normally positioned LBT (Fig 3c) (9). Scanning the entire length of the groove longitudinally to look for the fibrillar

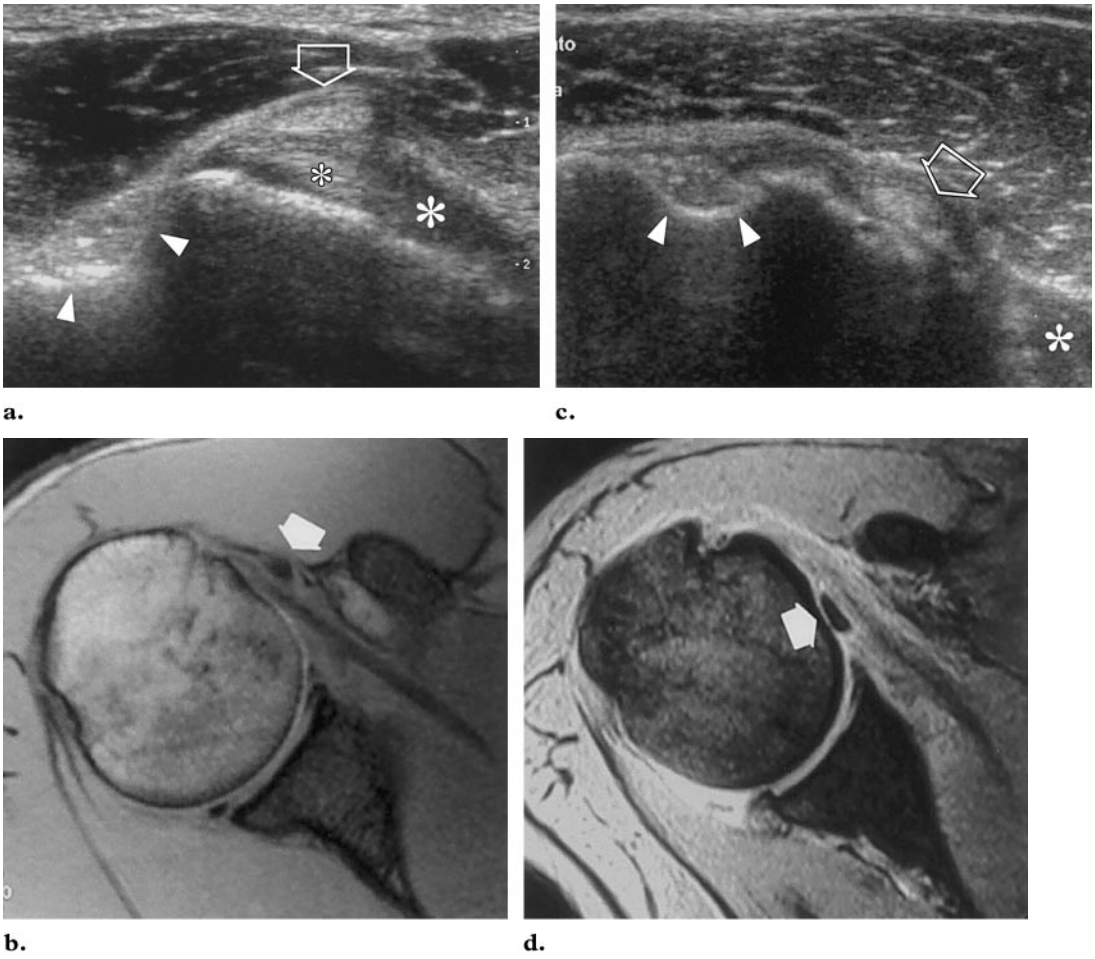

Figure 3. Biceps tendon dislocation. **(a, b)** Intact subscapularis tendon in a 27-year-old man with biceps tendon instability. Transverse 12–5-MHz US image **(a)** and corresponding gradient-recalled-echo (GRE) MR image (repetition time msec/echo time msec/flip angle = 400/12/90°) **(b)** demonstrate the biceps tendon (arrow) displaced superficial to the intact subscapularis tendon (∗ in **a**). Note that the intertubercular sulcus (arrowheads in **a**) is obtuse. **(c, d)** Full-thickness tear of the subscapularis tendon in a 58-year-old man with impingement syndrome. On a transverse 12–5-MHz US image **(c)** and corresponding GRE MR image (550/15/25°) **(d)**, the torn subscapularis tendon (∗ in **c**) is retracted from its normal attachment point on the lesser tuberosity, and the biceps tendon (arrow) is dislocated medially out of the groove (arrowheads in **c**).

pattern of the LBT, which is not seen in scar tissue, may help increase the examiner's confidence (1). In intermittent instability, a "to-and-fro" medial displacement of the tendon out of the groove is reported during maximal external and internal rotation of the arm (10). The entire length of the humeral groove should also be examined with transverse imaging to determine the osseous anatomy of the groove (11). In fact, a congenital shallow intertubercular sulcus (<3 mm deep) with a flat medial wall intrinsically predisposes to LBT instability (Fig 3a).

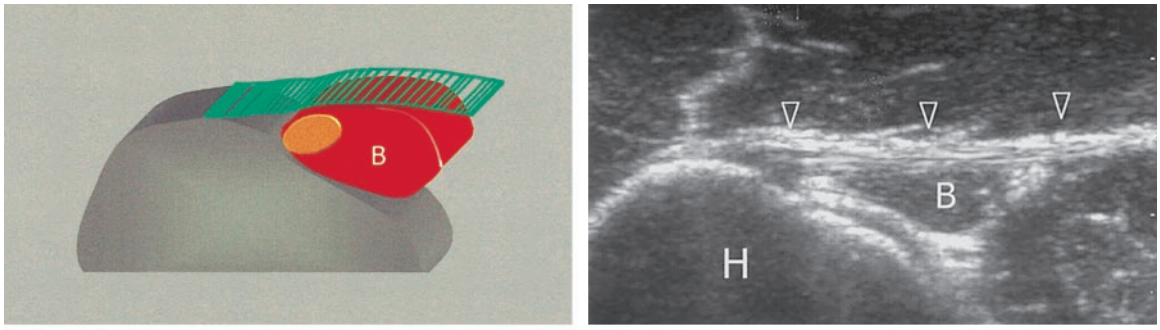

a. b.

Figure 4. Pectoralis major tendon. **(a)** Schematic illustrates the relationship of the pectoralis major tendon (green) to the myotendinous junction of the biceps (*B*). The biceps muscle and biceps tendon are shown in red and orange, respectively. **(b)** Corresponding transverse 12–5-MHz US image obtained distal to the humeral tuberosities shows the pectoralis major tendon (arrowheads), which crosses the myotendinous junction of the biceps tendon (*B*) on its anterior aspect to insert onto the humeral shaft (*H*).

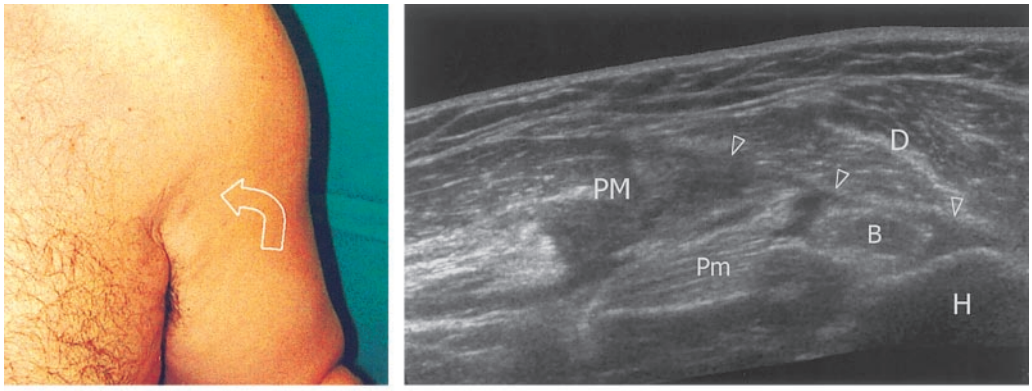

a. b.

Figure 5. Pectoralis major tendon tear in a 37-year-old man who presented with pain after attempting to catch a heavy object. **(a)** Clinical photograph shows a palpable defect (arrow) in the anterior wall of the left axilla. **(b)** Transverse extended-field-of-view 12–5-MHz US image reveals hypoechoic fluid that fills the bed of the ruptured pectoralis major tendon (arrowheads). Note the medial retraction of the belly of the pectoralis major muscle (*PM*) and the anterior displacement of the myotendinous junction of the biceps tendon (*B*), which appears to be surrounded by fluid. *D* = deltoid muscle, *H* = humerus, *Pm* = pectoralis minor muscle.

Farther distal to the humeral tuberosities, the main stabilizing structure of the LBT is the tendon of the pectoralis major muscle. This flattened tendon crosses anterior to the myotendinous junction of the LBT and inserts into the lateral lip of the intertubercular groove. At US, the pectoralis major tendon is identified dorsal to the deltopectoral groove (Fig 4). Rupture of this tendon is quite uncommon and occurs at either the myotendinous or teno-osseous junction (12). In complete tears, US findings include either a wavy appearance or nonvisualization of the tendon, depending on the site of the tear (Fig 5). The presence of hypoechoic fluid in the tendinous bed related to hematoma can help in making the diagnosis. The LBT and its myotendinous junction are surrounded by fluid and may appear elevated from the humerus.

Glenohumeral Joint

US is generally not appropriate for the evaluation of patients with GHJ instability. However, a scanning technique for documenting the presence, direction, and extent of glenohumeral translation has been described in patients with posterior shoulder subluxation or dislocation (13). With

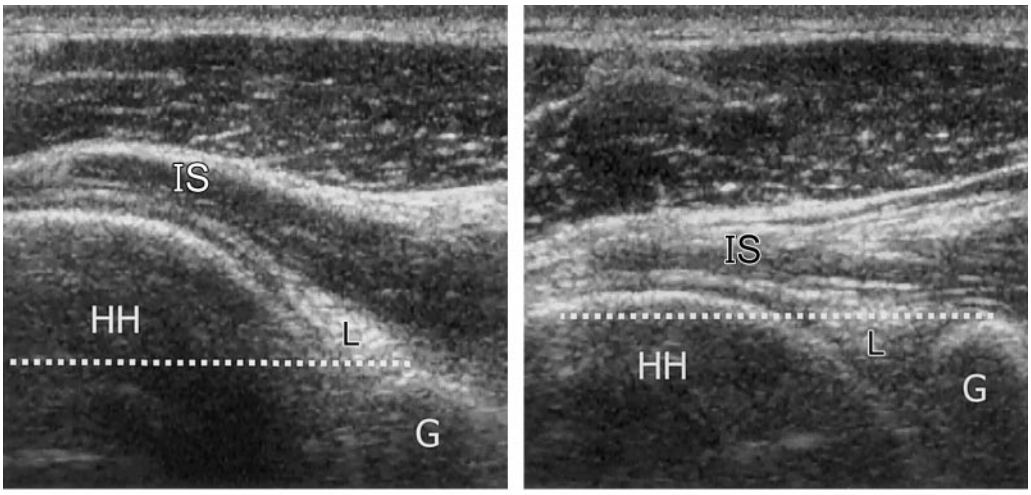

a. b.

Figure 6. Posterior GHJ instability in a 17-year-old girl with posterior voluntary subluxation. *IS* = infraspinatus tendon, *L* = posterior labrum. **(a)** Transverse 12–5-MHz US image obtained over the posterior right shoulder during subluxation shows that the humeral head (*HH*) is more exposed and posterior to the level of the bony glenoid (*G*) (dotted line). **(b)** US image obtained after reduction of the subluxation shows the humeral head (*HH*) and the glenoid (*G*) in exact apposition.

the examiner standing behind the patient, transverse scans should be obtained over the posterior GHJ to measure the distance between the dorsal rim of the bony glenoid and the tip of the humeral head. In voluntary subluxation, the patient is examined in different positions (neutral, 90° flexion, abduction, external rotation), including the position in which the patient perceives that the shoulder has become subluxated. The measured glenohumeral distances are compared for the affected shoulder and the healthy one: Differences greater than 20 mm indicate dislocation, whereas differences of 12 to 18 mm indicate subluxation (Fig 6).

An attempt can also be made with US to detect a variety of instability injuries that affect the glenoid labrum and the bone. The fibrocartilaginous labrum can be visualized at US as a triangular, homogeneously hyperechoic structure that caps the bony rim of the glenoid (14). A thin (<2-mm) hypoechoic zone at the base of the labrum is a normal finding. The anterior labrum is best scanned with curved-array transducers and low frequencies (as low as 5 MHz) with an anterior or axillary transverse approach performed either with the patient's arm in adducted position or with the patient supine and the arm abducted 90° with the elbow flexed (15). The posterior labrum is easily evaluated with posterior transverse scans of the GHJ at the level of the infraspinatus tendon; in contrast, the superior labrum is very difficult to see. Changes in the shape of the labrum can be observed in different rotations of the arm. A more pointed appearance is noted when traction is exerted on the labrum by the capsule (during external rotation for the anterior labrum). In general, the labrum is visualized more easily when it is surrounded by joint effusion. In anterior shoulder instability, the main criteria for anterior labral tear are an enlarged (>2-mm) hypoechoic zone at the base of the labrum, a truncated shape or absence of the labrum, and abnormal motility of the labrum at dynamic imaging, whereas an altered labral echogenicity seems to represent an inaccurate finding (15,16). On the other hand, a small, altered labrum indicates degenerative changes (15,17). In selected groups of young patients with acute traumatic or recurrent anterior shoulder dislocation, US is reported to have a sensitivity of 88%–95% and a specificity of 67%–100% in the diagnosis of labral tears (15). We believe that US has a promising role in the evaluation of the labrum, particularly in excluding labral tears when the labrum appears normal. Despite having limitations in the assessment of the anterior glenoid, US may occasionally demonstrate fragmentation of the anteroinferior rim, a finding that represents a Bankart lesion, as a V-shaped bone defect over the anterior aspect of the glenoid (15).

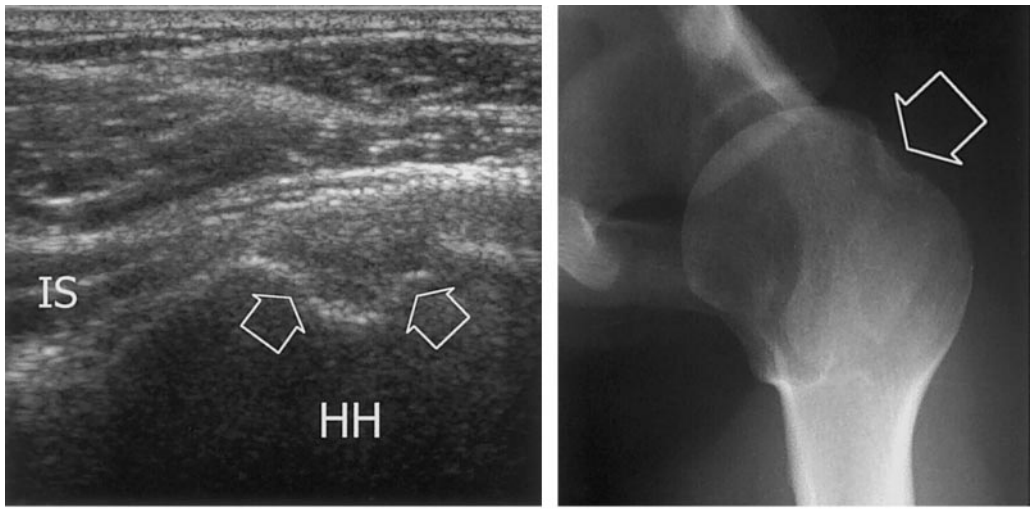

a. b.

Figure 7. Hill-Sachs lesion in a 47-year-old man with recurrent anterior shoulder instability. **(a)** Transverse 12–5-MHz US image obtained over the posterior shoulder reveals a wide, deep, and irregular grooved defect (arrows) of the humeral head (*HH*). *IS* = infraspinatus muscle. **(b)** Radiograph helps confirm the presence of a Hill-Sachs lesion (arrow).

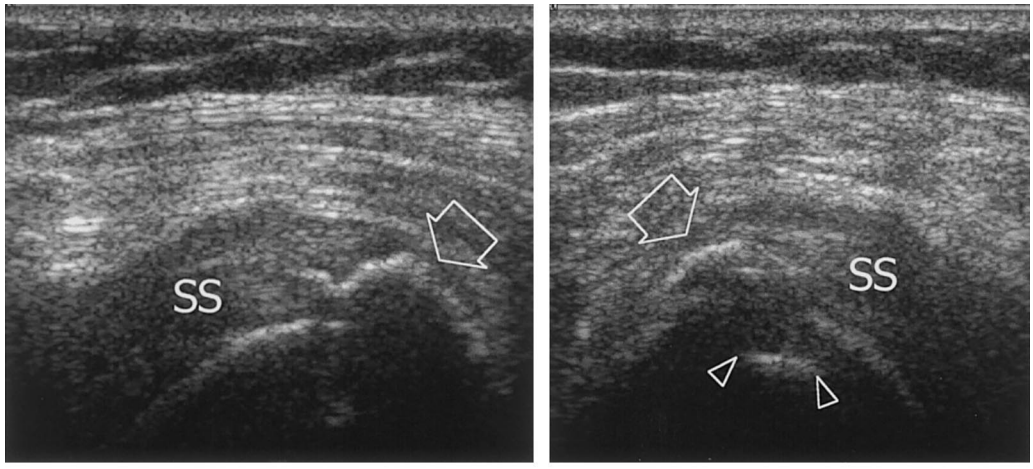

a. b.

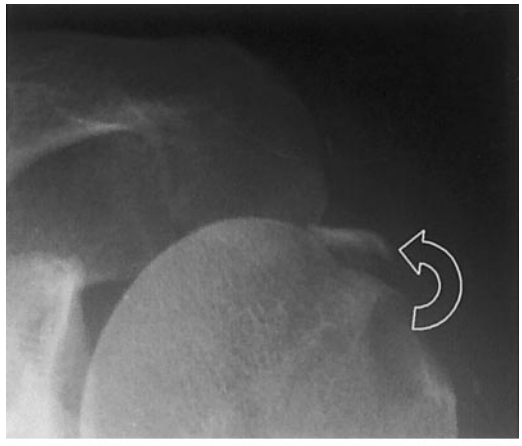

c.

Figure 8. Avulsion fracture of the greater tuberosity in a 32-year-old man with anterior shoulder instability. **(a, b)** Longitudinal **(a)** and transverse **(b)** 12–5-MHz US images demonstrate interruption of the continuity of the humeral surface (arrowheads in **b**) and a small fragment of bone (arrow) displaced superiorly into the supraspinatus tendon (*SS*). **(c)** Radiograph helps confirm the presence of an avulsion fracture (arrow).

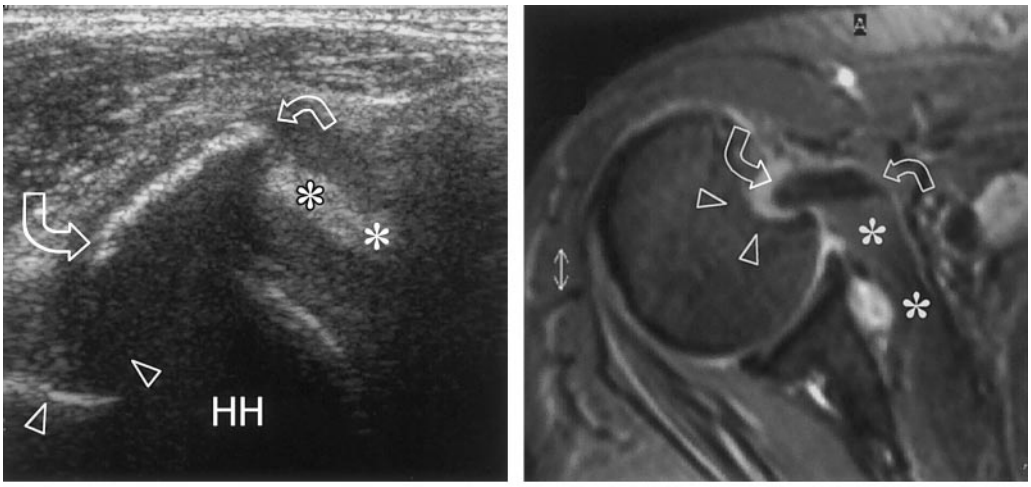

a. b.

Figure 9. Avulsion fracture of the lesser tuberosity in a 54-year-old woman with posterior shoulder instability. **(a)** Transverse 12–5-MHz US image obtained over the anterior shoulder shows a large fleck of bone (arrows) avulsed from the humeral head (*HH*). Note the deep defect (arrowheads) on the anterior surface of the humerus and the continuity of the avulsed bone with the subscapularis tendon (*). **(b)** Corresponding GRE MR image (500/15/20°) shows the avulsed bone fragment (arrows), the humeral defect (arrowheads), and the subscapularis tendon (*).

US is more reliable in the detection of other osseous injuries that accompany GHJ instability, such as Hill-Sachs and McLaughlin fractures and avulsions of the tuberosities. Hill-Sachs deformity is an osteochondral compression fracture located on the posterolateral humeral head that occurs in anterior shoulder dislocation. The fracture is created when the posterolateral humeral head strikes the anteroinferior glenoid rim during dislocation. US has a reported sensitivity of 91%–100%, a specificity of 89%–100%, and an accuracy of 84%–94% in detecting this lesion (18–20). The posterolateral shoulder should be examined in a transverse plane. A Hill-Sachs lesion appears as a shallow wedge-shaped defect of the hyperechoic bony contour of the humeral head at the point where the infraspinatus inserts into the greater tuberosity (Fig 7). The size and shape of the fracture can easily be assessed with US. It is important not to confuse a Hill-Sachs lesion with either the surface erosions of the humeral head secondary to rotator cuff tendinopathy, which are usually smaller and more superficial, or the more caudal normal depression of the humeral neck (2). A similar impaction fracture of the anterior surface of the humeral head, commonly referred to as trough fracture or McLaughlin fracture, is encountered in posterior GHJ dislocations. In such cases, US can demonstrate a bone defect on the anterolateral surface of the humeral head deep to the subscapularis tendon.

Avulsions of the tuberosities can also be encountered in shoulder instability. Greater tuberosity fractures may arise from an acute distraction avulsion injury caused by the supraspinatus tendon. When undisplaced, these fractures appear as a break or step-off deformity of cortical bone at the notch between the humeral head and the greater tuberosity or at the junction of the humeral shaft and the anatomic neck of the humerus, thereby suggesting an elevated fragment (21). The uplifted fragment may be angled or overlapping, and the contiguous portion of the supraspinatus tendon appears abnormally thickened and heterogeneous due to edema and contusion (Fig 8). Visualization of a well-demarcated defect on the surface of the greater tuberosity can help avoid misdiagnosis as calcifying tendinitis. Avulsions of the lesser tuberosity can also be found in posterior shoulder dislocations as a result of subscapularis traction (Fig 9). However, conventional radiographs are necessary to confirm these findings.

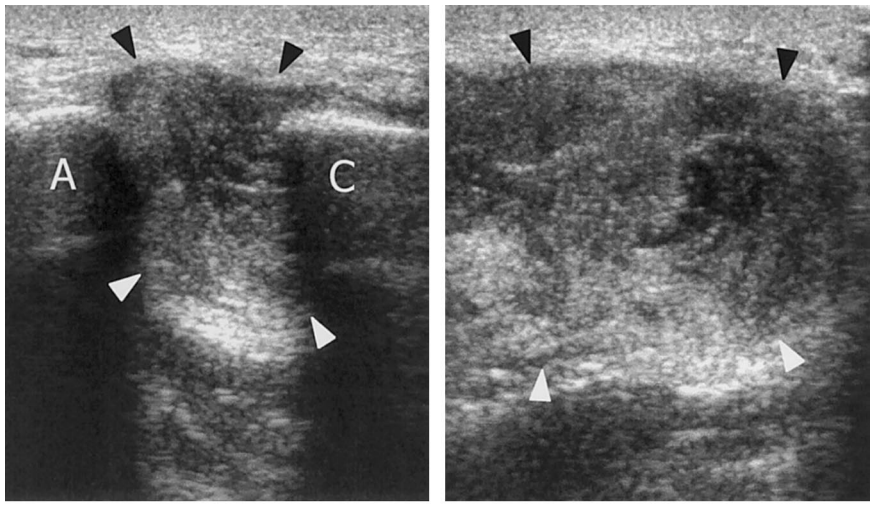

a. **b.**

Figure 10. Mild ACJ sprain in a 42-year-old woman with posttraumatic shoulder pain. Coronal **(a)** and sagittal **(b)** 13–10-MHz US images reveal a widened, echogenic joint space (arrowheads). *A* = acromion, *C* = clavicle.

Acromioclavicular Joint

Subluxation or dislocation of the ACJ may be a source of shoulder pain that is often confused for a rotator cuff tear because of the proximity of this joint to the tendons of the rotator cuff. US is more sensitive than conventional radiography in detecting low-grade sprains. In such cases, the superior capsule and ligament may become prominent, and the joint cavity appears widened and distended by hematoma or fluid (Fig 10). When the ACJ is more severely injured, an upward displacement of the distal end of the clavicle can be appreciated. In high-grade dislocations, a hypoechoic hematoma in the soft tissues between the clavicle and the coracoid process may be considered as an indirect sign of injured coracoclavicular ligaments.

Although US is not routinely used in screening for ACJ separation, some attempts have been made with this modality to quantify acute and chronic ACJ instability of varying severity according to the radiographic scale described by Tossy et al (22). The width of the joint is measured with a coronal approach and compared with that of the contralateral ACJ. Measurements should be taken with the patient letting the arms hang down and holding a 10-kg weight in each hand. An acromioclavicular index (AC index) is then calculated by dividing the ACJ width on the normal side by that on the injured side. In Tossy-I injury, the ACJ width was no more than 6 mm and the AC index was 1.0; patients with Tossy-II instability had a mean ACJ width of 10.2 mm on the injured side and an AC index of 0.5; and patients with Tossy-III instability and an indication for surgery had a mean ACJ width of 22.3 mm on the injured side and an AC index of less than 0.25 (23). Additional measurements of the coracoclavicular distance may increase diagnostic confidence.

Osteolysis of the clavicle may occur from several weeks to several years after the ACJ trauma. This process is self-limiting, with gradual reparative changes occurring over a period of 4–6 months (24). At US, the resorption of the clavicular tip manifests as irregular cortical erosions associated with joint space widening, joint effusion,

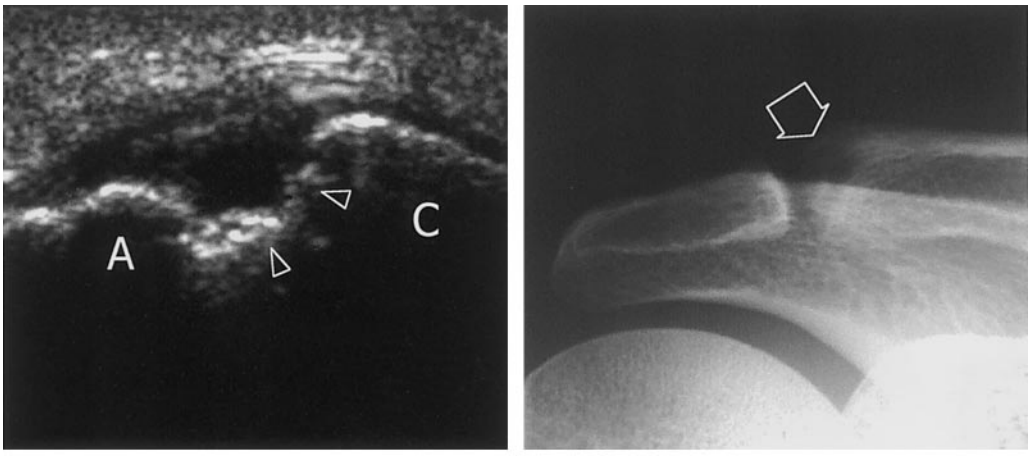

a. b.

Figure 11. Posttraumatic osteolysis of the clavicle in a 25-year-old man with a 6-month history of posttraumatic pain and tenderness over the ACJ. **(a)** Coronal 10–5-MHz US image demonstrates irregular erosion (arrowheads) of the distal end of the clavicle (*C*). *A* = acromion. **(b)** Radiograph helps confirm the presence of osteolysis (arrow).

and soft-tissue swelling, whereas the acromion remains intact (Fig 11). Clavicular osteolysis should be included in the differential diagnosis when a patient experiences chronic pain or soft-tissue swelling beyond the acute phase of the injury.

Arthropathies and Bursites

US is commonly used to examine synovial disorders. Knowledge of the soft-tissue anatomy and of the technique for examining the main synovial recesses and bursae around the shoulder girdle, particularly the recesses of the GHJ and the subacromial-subdeltoid (SA-SD) bursa, is essential for the US examiner to avoid misdiagnoses and pitfalls in the interpretation of pathologic findings.

The GHJ capsule extends from the boundaries of the labrum and glenoid rim to the neck of the humerus. To allow a wide range of arm movements, the capsule is lax and redundant. In normal states, the joint space is a potential space that is not visible at US; when the joint space contains effusions, US may delineate fluid in the dependent axillary pouch and in three main synovial recesses: the posterior and anterior recesses and the sheath of the LBT. Fluid in the axillary pouch is evaluated on posterior transverse scans obtained below the inferior edge of the teres minor muscle. The transducer is moved upward, and the posterior recess is then examined deep to the infraspinatus tendon. Changes in the appearance of a fluid collection in this recess can be appreciated when the arm is externally rotated, which reduces the tension on the posterior structures. Increased fluid in the posterior recess splays the infraspinatus tendon and creates a hypoechoic crescent around the posterior labrum (Fig 12a). Evaluation of the anterior recess is more complex due to the deep location of the recess and often requires a lower-frequency curvilinear array probe and careful scanning technique. When fluid is present, it can be appreciated on transverse scans as a hypoechoic halo that surrounds the labrum. An opening in the anterior capsule creates a communication between the joint and the superior subscapularis recess. This small recess has a saddle shape; it originates between the anterior neck of the scapula and the subscapularis tendon, overlying and then descending anterior to the

Figure 12. Fluid collections in the SA-SD bursa. **(a)** Transverse 12–5-MHz US image obtained over the posterior shoulder reveals a bursal fluid collection (*) overlying the infraspinatus tendon (*IS*). Note the coexistent joint effusion in the posterior recess (☆) deep to the infraspinatus tendon. *G* = glenoid, *HH* = humeral head. **(b)** Coronal 12–5-MHz US image obtained over the lateral shoulder shows a bursal fluid collection (*) just inferior to the greater tuberosity (*GT*) and distal to the insertion of the supraspinatus tendon (*SS*). **(c)** Transverse 12–5-MHz US image obtained over the anterior shoulder demonstrates a bursal fluid collection (*) that extends superficial to the bicipital groove. Note the lack of fluid in the underlying biceps tendon sheath (arrow), a finding that reflects the absence of communication between the SA-SD bursa and the GHJ. *GT* = greater tuberosity, *LT* = lesser tuberosity.

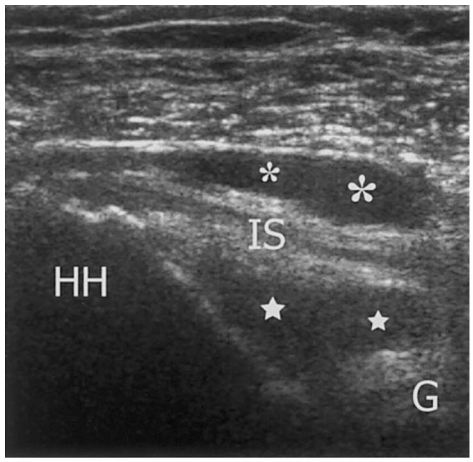

a.

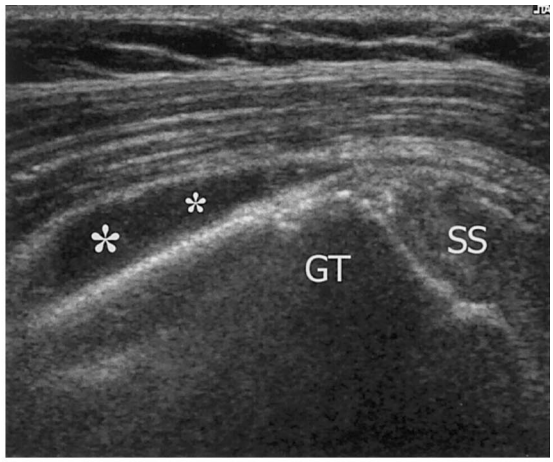

b.

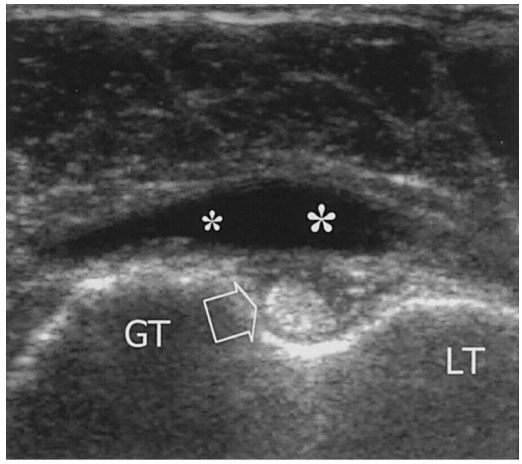

c.

superior tendon edge. The superior subscapularis recess does not usually extend beyond the tip of the coracoid process unless a large, intraarticular effusion causes considerable distention of the joint cavity. Sagittal scans can better depict this recess if it is distended by fluid. The superior subscapularis recess should not be confused with the larger subcoracoid bursa, which extends more caudally and does not normally communicate with the GHJ but may communicate with the SA-SD bursa (25). The subcoracoid bursa extends deep to the conjoint tendon of the short head of the biceps and the coracobrachial muscle and may contain a large amount of fluid in cases of anterior rotator cuff tears. It is best examined by scanning just inferior and medial to the coracoid process with the patient's arm adducted. Furthermore, the synovial membrane extrudes at the level of the rotator cuff interval to form the LBT sheath. This sheath surrounds the LBT down to approximately 4 cm beyond the distal end of the bicipital groove. Because the LBT sheath is merely an extension of the joint cavity, joint effusion can lead to fluid in the sheath. Fluid as a result of an isolated biceps tendinitis is rare.

In adhesive capsulitis ("frozen shoulder"), a clinical syndrome characterized by pain and severely restricted joint movement, thickening and fibrosis of the joint capsule and synovium lead to reduced articular volume capacity. Although US

Figure 13. Rheumatoid arthritis in a 62-year-old woman with long-standing disease. **(a)** Transverse 12–5-MHz US image obtained over the posterior shoulder reveals a hypoechoic soft-tissue mass that represents synovial pannus within the posterior recess (arrowheads). In addition, there is a defect (arrow) of the posterior humeral head (*HH*), a finding that represents erosion. *G* = glenoid. **(b)** Corresponding GRE MR image (500/15/20°) demonstrates the soft-tissue mass (arrowheads).

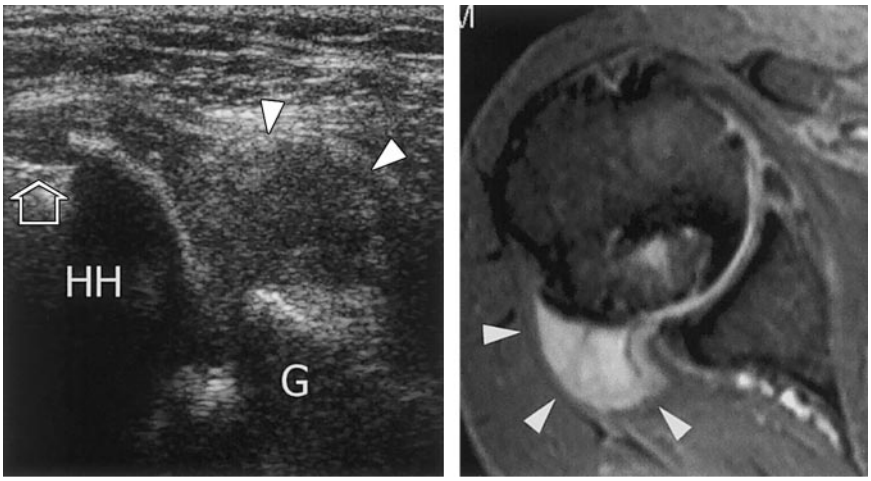

a. **b.**

cannot depict adhesions or help measure the restriction of the joint cavity, the diagnosis may be suggested at dynamic scanning by either restriction of sliding movements of the supraspinatus tendon underneath the acromion during arm abduction or persistent visualization of the supraspinatus tendon during lateral elevation of the arm (26). Minimal synovial inflammation may be an associated finding.

The SA-SD bursa covers a large area of the shoulder. It extends medially to the coracoid process and anteriorly to cover the bicipital groove, whereas its lateral and inferior boundary is more variable and extends to approximately 3 cm below the greater tuberosity (27). The normal synovial membrane of the bursa cannot be visualized at US. The SA-SD bursa appears as a 2-mm-thick complex consisting of an inner layer of hypoechoic fluid between two layers of hyperechoic peribursal fat (28). Fluid collections tend to accumulate in the most dependent portions of the bursa and, more commonly, along the lateral edge of the greater tuberosity, producing a typical "teardrop" appearance (Fig 12b) (28). Small amounts of fluid can go unnoticed if this portion of the bursa is not examined or if fluid is squeezed away by exerting excessive pressure with the probe. More abundant fluid collections fill the bursa anterior to the bicipital groove and must not be confused with intraarticular fluid contained within the LBT sheath (Fig 12c).

Inflammatory Diseases

Rheumatoid arthritis usually involves not only the GHJ, but also the ACJ and the synovial bursae around the shoulder. US has been shown to reveal synovitis in the early stages of disease, when no radiographic changes are yet evident, as well as to help differentiate between synovial hypertrophy and effusions (Fig 13) (29,30). In a selected group of patients with symptomatic disease, US assessment of synovitis has shown SA-SD bursitis to be the most common finding, occurring in up to 69% of cases, followed by GHJ involvement in 58% and biceps tendinitis in 57% (31). Overall, no correlation was observed between these findings and either duration or stage of disease according to radiographic criteria for the evaluation of hand or wrist joints. A quantitative assessment of synovitis may be attempted by measuring the widest distance between the humeral head and the joint capsule in the axillary pouch and posterior recesses (29,31). It may be difficult to distinguish fluid from the pannus in the posterior recess because graded compression does not always

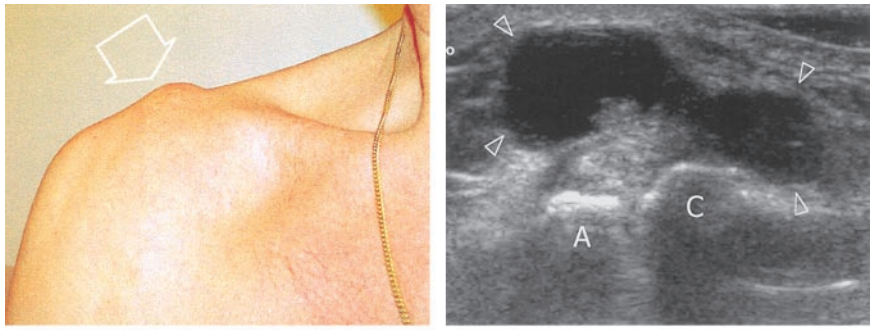

a. b.

Figure 14. ACJ cyst in a 68-year-old man with a chronic rotator cuff tear. **(a)** Clinical photograph demonstrates a soft-tissue mass (arrow) that arises over the ACJ. **(b)** Coronal 12–5-MHz US image reveals a cystic mass (arrowheads) that arises from the ACJ. *A* = acromion, *C* = clavicle.

squeeze the fluid away owing to increased intraarticular pressure. Color and power Doppler US may be used to assess the activity of the inflammatory process by depicting hyperemic flow within the synovial tissue (29). However, the reliability of these findings seems inadequate for objective assessment, especially when color Doppler US is used to evaluate response to therapy. It is possible that US contrast agent will have a role in this setting. Along with synovium, US is able to reveal bone erosions, which usually appear as cortical defects filled with hypoechoic pannus (30). Loss of definition and thinning of the articular cartilage can be demonstrated in advanced disease as well. Because it allows clear visualization of the needle tip, US is excellent for imaging-guided synovial needle biopsy as well as for intraarticular injection of corticosteroids, thereby avoiding the risks of inadvertent intratendinous steroid injection. US-guided needle placement is more accurate and less painful than needle placement without US guidance. US has also been used to investigate the structures involved by the inflammatory process in polymyalgia rheumatica (32–34). Most studies report that bursitis is seen considerably less frequently than GHJ synovitis (14%–16% versus 57%–66% of cases, respectively) in this disease (32,33).

Degenerative and Infiltrative Disorders

Degenerative osteoarthritis of the GHJ is most often associated with chronic massive disruption of the rotator cuff. US findings include bone changes related to the superior subluxation of the humerus, formation of osteophytes along the inferior margin of the humeral head, bone spurring in the tuberosities and at the bicipital groove, and joint effusion. Superior humeral subluxation may be identified at coronal US as a reduced acromiohumeral distance. The humeral head shows loss of the hypoechoic layer of articular cartilage and bone irregularities; the greater tuberosity has a smooth appearance and blends with the humeral epiphysis. In these circumstances, detection of the bicipital groove can be problematic. Reduced thickness of the acromion may also be observed. The subluxation of the humerus may lead to secondary damage of the inferior ACJ capsule and passage of joint fluid through the ACJ, producing a cyst in the soft tissues at the superior aspect of the shoulder ("geyser sign"), a finding that may be considered pathognomonic for long-standing massive rotator cuff tears (Fig 14) (26). During passive movements of the arm or exertion of pressure on the cyst with the probe, debris may be seen moving to and fro across the ACJ. In shoulder osteoarthritis, the progressive disintegration of the articular surfaces leads to the formation and release of intraarticular loose bodies which, once freed into the joint cavity, can progressively worsen the damage to the joint surfaces. Osteochondral loose bodies usually remain trapped in the most dependent portions of the GHJ, such as the axillary pouch and the LBT sheath (Fig 15). Most of these loose bodies appear as hyperechoic areas with posterior acoustic shadowing. In some cases, however, a thin layer of hypoechoic cartilage may be seen overlying the echogenic interface of the subchondral bone (35). The size and

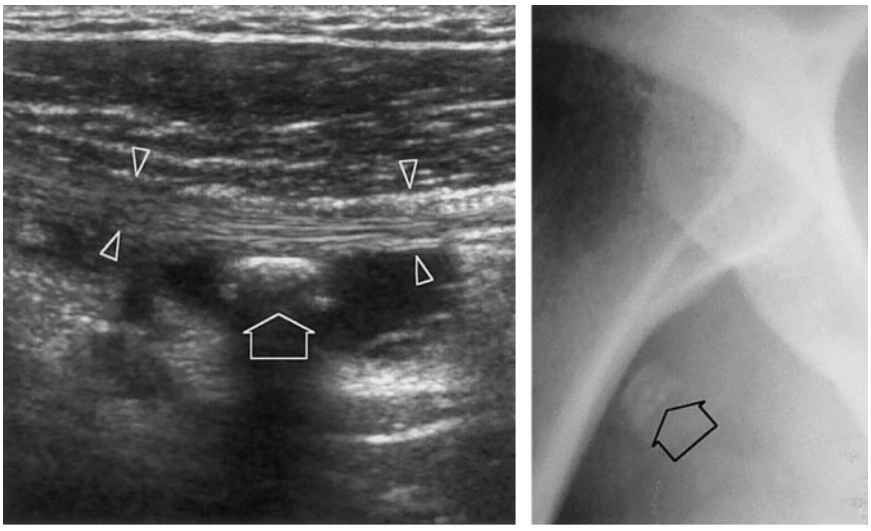

a. b.

Figure 15. Intraarticular loose body in a 45-year-old woman. **(a)** Longitudinal 12–5-MHz US image of the shoulder obtained at the level of the sheath of the LBT (arrowheads) demonstrates a loose body (arrow) surrounded by anechoic fluid in the synovial space. **(b)** Corresponding radiograph shows the fragment with a typical laminated concentric appearance (arrow).

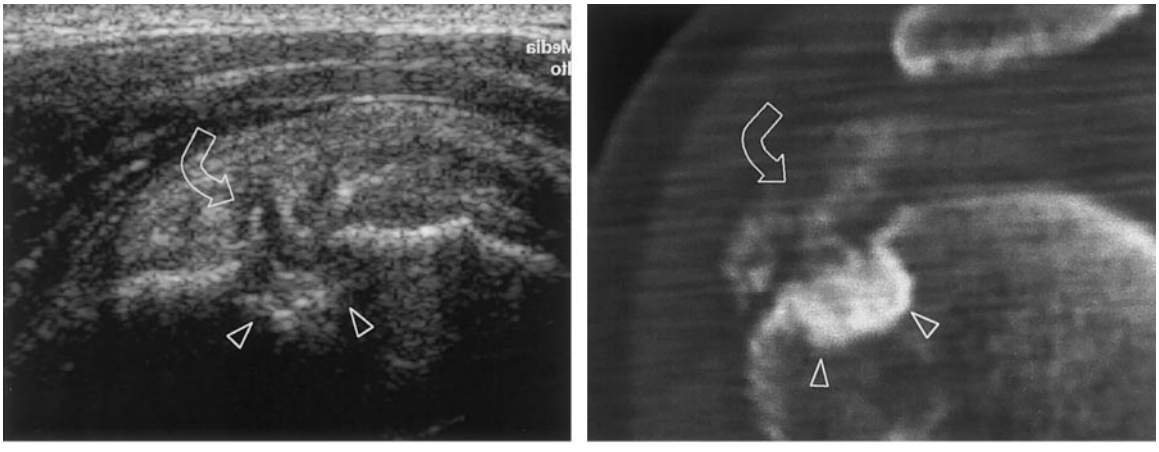

a. b.

Figure 16. Intraosseous loculation of calcifying tendinitis in a 54-year-old man with boring shoulder pain. **(a)** Longitudinal 12–5-MHz US image of the supraspinatus tendon demonstrates calcific slurry (arrow) within the tendon. The calcific material extends into a deep cavity within the greater tuberosity (arrowheads). **(b)** Corresponding CT scan demonstrates the calcifications (arrow) and the cavity within the greater tuberosity (arrowheads).

position of a fragment can be reliably evaluated with US, but the exact number of fragments cannot always be established.

Other conditions that lead to the rapid development of joint destruction with deposition of calcium apatite crystals cannot be specifically identified in patients with rotator cuff osteoarthritis. On the other hand, US is sensitive in depicting the deposition of pyrophosphate crystals in the cartilage of the humeral head in patients with chondrocalcinosis (36). These crystals appear as a blurry hyperechoic line that runs parallel to the cartilage surface. In patients with calcifying tendinitis, the calcific deposit may extrude either into the bone or within the SA-SD bursa. Intraosseous calcific material can be visualized as a hypoechoic notch in the greater tuberosity that contains scattered foci of increased echogenicity (Fig 16). In

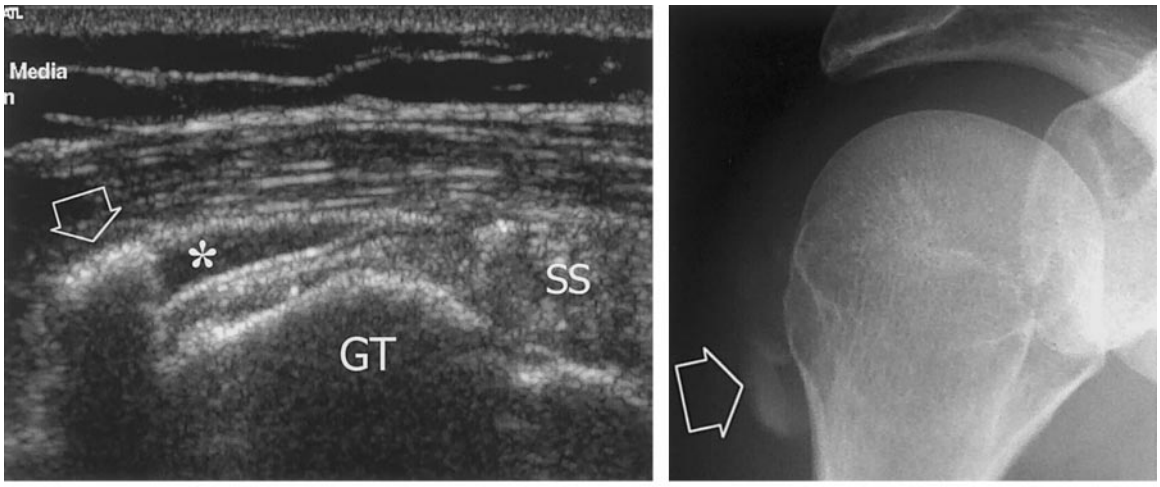

a. b.

Figure 17. Intrabursal rupture of calcifying tendinitis in a 46-year-old woman with severe shoulder pain and tenderness. **(a)** Coronal 12–5-MHz US image obtained over the lateral shoulder reveals a thickened SA-SD bursa that contains fluid (*) and calcified material (arrow) just inferior to the greater tuberosity (*GT*) and distal to the insertion of the supraspinatus tendon (*SS*). **(b)** Corresponding radiograph shows calcified material (arrow) that lies in the dependent lateral portion of the SA-SD bursa.

intrabursal rupture, calcific slurry may manifest as a fluid-calcification level in the dependent pouch of a thickened bursa (Fig 17). Although subtle, these findings may help explain the severe pain that usually accompanies the extrusion of calcium. Markedly echogenic thickening of the synovium (especially in the SA-SD bursa), periarticular nodules within the soft tissues surrounding the rotator cuff, and bone erosions may be observed in dialysis-related shoulder arthropathy, findings that reflect amyloid deposition of β_2-microglobulin as an amyloid protein (37–39). US features of shoulder amyloidosis are varied and also include a heterogeneous and thickened rotator cuff, especially with involvement of the supraspinatus and subscapularis tendons. US allows early diagnosis based on these findings and should be useful in disease follow-up.

Infections

Septic arthritis of the GHJ mainly results from the inadvertent introduction of bacteria during nonsterile iatrogenic procedures such as arthrocentesis or injection of corticosteroids into the joint. Although US is sensitive in the detection of GHJ effusion, particularly in the shoulder in which physical examination is less reliable, US findings usually do not allow differentiation of a noninfected joint effusion from septic arthritis (40).

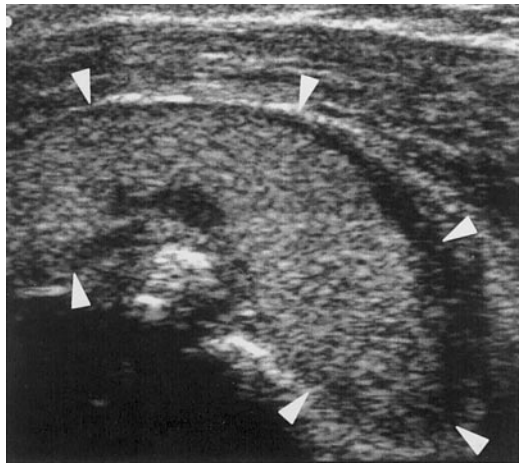

Figure 18. Septic bursitis in a 37-year-old woman who presented with increasing shoulder pain and swelling after undergoing corticosteroid injection. Coronal 12–5-MHz US image obtained over the lateral shoulder demonstrates an SA-SD bursa (arrowheads) that is grossly distended by highly echogenic fluid. Aspiration revealed purulent material.

Definitive diagnosis requires analysis of the fluid, possibly aspirated under US guidance. A large-bore (16–18-gauge) needle is ideal for this purpose because purulent material can be too thick and viscous to be aspirated with a small needle. The needle should be inserted at the midglenohumeral level and directed into the posterior recess through the infraspinatus. Septic arthritis is usually not associated with bursal infection unless a

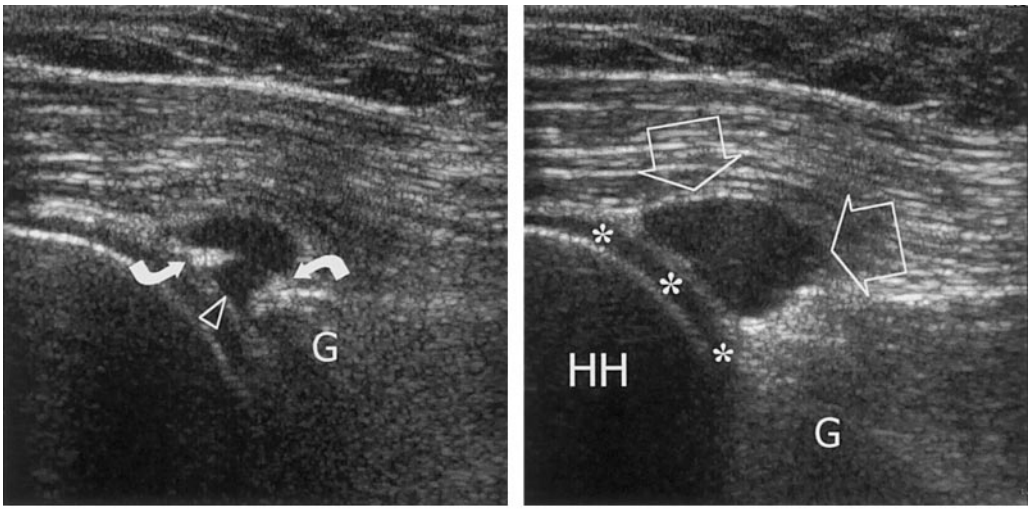

a. b.

Figure 19. Paralabral ganglion cyst. Coronal 12–5-MHz US images of the inferior GHJ show an abnormal hypoechoic area (arrowhead in **a**) in the inferior labrum (arrows in **a**) that represents an inferior labral tear. The tear is contiguous with a small paralabral cyst (arrows in **b**) that extends inferiorly. Note the humeral head (*HH*) covered by hypoechoic articular cartilage (∗ in **b**). *G* = glenoid.

full-thickness rotator cuff tear is present; however, these two entities may overlap to such an extent that clinical differentiation may be difficult. At US, an infected SA-SD bursa may appear distended by a complex fluid collection that contains debris and septa (Fig 18) (40,41). The bursal walls may be thickened, and peribursal hypoechoic strands that represent edema in the surrounding soft tissues may be an associated finding. Although color and power Doppler US may depict hyperemic flow in the synovial walls and around the bursa, this finding is not considered specific for infectious disease. When the joint recesses are fluid free, US is reliable in making a correct diagnosis of isolated bursal involvement, thus obviating arthrocentesis with its potential complications (41). US-guided aspiration of the infected bursa may help avoid inadvertent contamination of the underlying sterile joint caused by traversing the infected bursa with the needle. In sepsis of the ACJ, US is useful for excluding involvement of the adjacent SA-SD bursa and GHJ. The main US findings are superior bulging of the joint capsule, widening of the joint space with erosion of the bony edges, and debris moving freely within the joint space (42). Although aspiration of the infected joint can easily be performed without imaging guidance, US allows the procedure to be performed more confidently.

Nerve Entrapment Syndromes

A torn labrum may be accompanied by the development of paralabral ganglion cysts. These cysts are somewhat similar to those associated with meniscal tears of the knee and may develop from the abnormal passage of joint fluid through the labrum. In the shoulder, paralabral cysts most commonly arise from the superior or posterior labrum as a consequence of a superolateral anterior-to-posterior tear or posterior instability, respectively. Rarely, they may extend from the anteroinferior glenoid. Posterior paralabral cysts can spread into the spinoglenoid notch, suprascapular notch, or both notches of the scapula, deep to the myotendinous junction of either the supraspinatus or infraspinatus muscle (43). Routine scanning of the posterior shoulder with low magnification is recommended for detecting these cysts owing to their deep location. US can help identify paralabral ganglion cysts as rounded or oval hypoechoic lesions with well-defined margins that remain relatively fixed in location and shape during shoulder movements (44). Occasionally, the neck of the ganglion can be visualized within the torn labrum (Fig 19). Progressive enlargement of paralabral cysts at these sites may indicate an

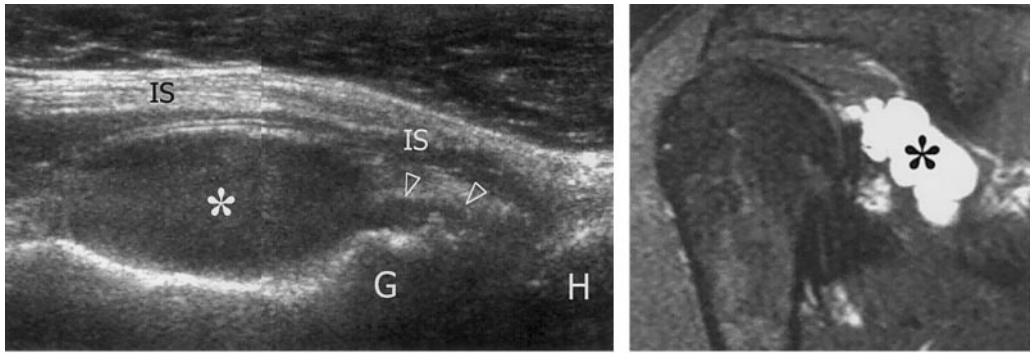

a. b.

Figure 20. Suprascapular nerve entrapment at the spinoglenoid notch in a 54-year-old man. Longitudinal 12–5-MHz US image obtained over the posterior shoulder **(a)** and corresponding coronal fat-saturated GRE MR image (700/15/20°) **(b)** reveal an oval cystic lesion (*) located deep to the infraspinatus tendon (*IS*) and medial to the glenoid (*G*), a finding that is consistent with a ganglion cyst. Note the thin neck of the cyst (arrowheads in **a**) directed toward the GHJ. *H* = humeral head.

entrapment neuropathy of the suprascapular nerve (Fig 20).

The suprascapular nerve descends from the suprascapular notch to the supraspinatus fossa, sending branches to supply the supraspinatus muscle, and then continues down into the spinoglenoid notch to supply the infraspinatus muscle. This anatomic layout may help explain the main characteristics of nerve dysfunction: If the ganglion expands in the supraspinous notch, it causes atrophy of both the supraspinatus and infraspinatus muscles; if the ganglion expands in the spinoglenoid notch, it leads to isolated atrophy of the infraspinatus muscle (45). The suprascapular nerve may occasionally be visualized at US in the spinoglenoid notch adjacent to the suprascapular artery. US can help identify the cyst and help assess degenerative changes in denervated muscles based on their loss in bulk and increased reflectivity due to replacement by fat. US may also help exclude tendon rupture. Needle aspiration of the ganglion can be attempted under US guidance (44,45). The reported success rate of this procedure is 86% (45).

Another compressive neuropathy in the posterior shoulder involves the axillary nerve (46). This nerve arises from the posterior cord of the brachial plexus near the level of the coracoid process. It passes along the inferolateral border of the subscapularis muscle, around which it winds to traverse the so-called "quadrilateral space" that lies in intimate contact with the inferior capsule, and supplies the teres minor and deltoid muscles (47). The quadrilateral space is delimited by the teres minor muscle superiorly, the teres major muscle inferiorly, the long head of the triceps muscle medially, and the humeral neck laterally. Axillary nerve compressive neuropathy most often occurs in association with fibrous bands in the quadrilateral space. It can be difficult to diagnose clinically, given that the relative contributions of the teres minor and infraspinatus muscles cannot be determined with certainty. However, space-occupying lesions, including paralabral cysts that extend from the inferior glenoid in association with a tear of the inferior labrum, may also result in such nerve entrapment (48). Although the axillary nerve is too small to be recognized at gray-scale US, color Doppler US can provide indirect information about its location by depicting flow signals from the adjacent posterior circumflex artery. Even without any detectable soft-tissue abnormality along the nerve course, selective atrophy of the innervated muscles in the absence of a tendon tear strongly supports the diagnosis of a nerve lesion (Fig 21).

Space-occupying Lesions

Superficial masses around the shoulder (eg, subcutaneous lipomas, ganglia) can generally be identified at US. However, deep-seated lesions may be difficult to recognize. The most common

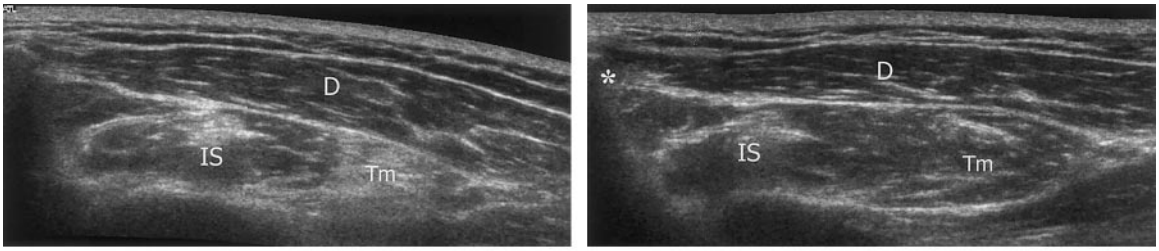

a. b.

Figure 21. Axillary nerve entrapment in a 24-year-old man with no obvious history of trauma. **(a)** Sagittal extended-field-of-view 12–5-MHz US image obtained over the posterior fossa demonstrates loss in bulk and increased echogenicity of the teres minor muscle (*Tm*), a finding that is consistent with fat atrophy. The infraspinatus muscle (*IS*) is preserved. *D* = deltoid muscle. **(b)** Corresponding US image obtained on the contralateral side shows a normal teres minor muscle (*Tm*) and infraspinatus muscle (*IS*). ∗ = spine of the scapula, *D* = deltoid muscle.

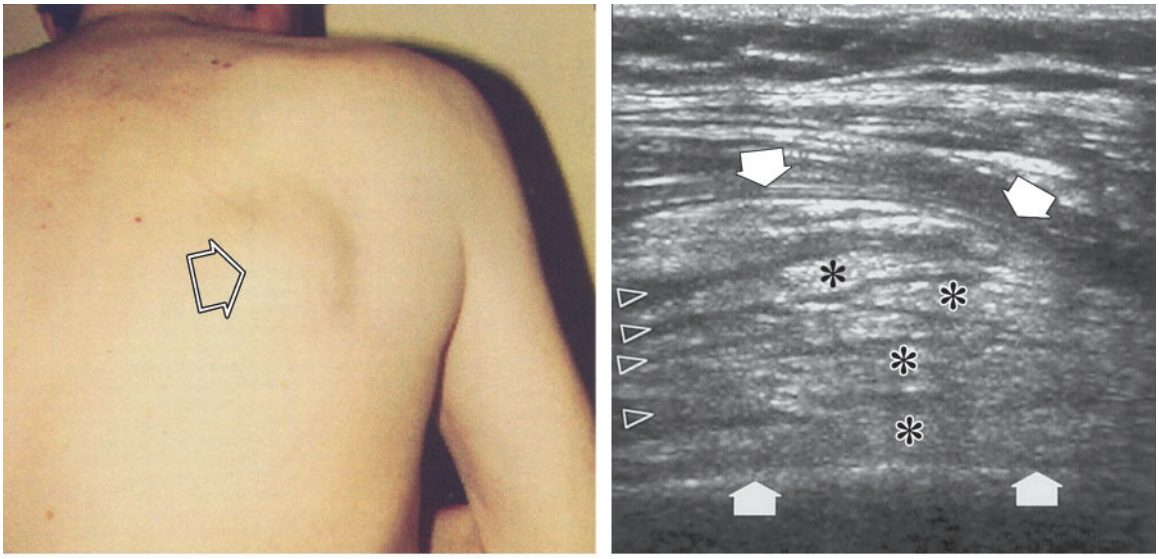

a. b.

Figure 22. Elastofibroma dorsi in a 46-year-old man with stiffness and clicking of the scapula. **(a)** Clinical photograph obtained with the patient's arm abducted shows a mass effect in the dorsum (arrow). **(b)** Transverse 12–5-MHz US image reveals an elastofibroma dorsi (arrows). The mass exhibits a typical striated appearance created by hypoechoic stripes of fat (arrowheads) on an echogenic background (∗), a finding that represents fibroelastic tissue.

of these lesions is elastofibroma dorsi, a reactive pseudotumor located in the subscapular region that is often bilateral and associated with hard manual labor. Elastofibromas appear as crescentic masses between the extrinsic back muscles and the costal plane. They are composed of alternating fatty and fibrous tissue planes, which gives the mass a multilayered appearance (49). At US, elastofibroma dorsi has a peculiar multilayered appearance created by interspersed linear and curvilinear hypoechoic strands (fatty tissue) against an echogenic background (the fibroelastic bulk of the mass) (Fig 22) (50). In the appropriate clinical setting, the US diagnosis of elastofibroma can obviate further imaging and biopsy.

Conclusions

As experience increases, high-resolution US is proving to be a rapid, low-cost, accurate means of assessing a spectrum of non–rotator cuff disorders that affect the shoulder girdle. In the setting of shoulder instability, dynamic US performed with varying degrees of patient arm rotation and joint stress maneuvers provides unique information

that cannot be obtained with other imaging methods by depicting subtle disorders such as intermittent dislocation of the biceps tendon. In posterior shoulder instability, a frequently missed diagnosis, US allows direct assessment of the extent of humeral head displacement, whereas in anterior shoulder dislocation it can help identify Hill-Sachs lesions and glenoid labrum tears. In the work-up of shoulder arthritis, US depiction of cortical erosions can support the choice of an aggressive therapy. Color and power Doppler US may also help differentiate active from fibrous pannus, thereby influencing treatment duration. In addition, US can be used to guide synovial biopsy and joint fluid aspiration if septic or microcrystalline arthritis is suspected clinically. Suprascapular or axillary nerve entrapment may be difficult to differentiate clinically from rotator cuff lesions. US has been shown to play a role in the diagnosis of these conditions. When a soft-tissue mass is evident in the shoulder area, US can help determine whether the mass is solid or cystic. Many shoulder masses (eg, ganglia, synovial cysts, lipomas, elastofibromas) have a pathognomonic location and appearance and can be clearly assessed with US apart from MR imaging.

Once adequate radiographs have been obtained to exclude apparent bone disorders, high-resolution US should be the first-line imaging modality in the assessment of non–rotator cuff disorders of the shoulder, assuming the study is performed with high-end equipment by an experienced examiner. More costly and invasive modalities such as MR imaging, CT arthrography, and MR arthrography should be reserved for bone marrow evaluation and preoperative assessment.

References

1. Teefey SA, Middleton WD, Yamaguchi K. Shoulder sonography: state of the art. Radiol Clin North Am 1999; 37:767–785.
2. Bouffard JA, Lee SM, Dhanju J. Ultrasonography of the shoulder. Semin Ultrasound CT MR 2000; 21:164–191.
3. Weishaupt D, Zanetti M, Tanner A, Gerber C, Hodler J. Lesions of the reflection pulley of the long biceps tendon: MR arthrographic findings. Invest Radiol 1999; 34:463–469.
4. Werner A, Mueller T, Boehm D, Gohlke F. The stabilizing sling for the long head of the biceps tendon in the rotator cuff interval: a histoanatomic study. Am J Sports Med 2000; 28:28–31.
5. Patton WC, McCluskey GM III. Biceps tendinitis and subluxation. Clin Sports Med 2001; 20:505–529.
6. Bennett WF. Subscapularis, medial and lateral head coracohumeral ligament insertion anatomy: arthroscopic appearance and incidence of "hidden" rotator interval lesions. Arthroscopy 2001; 17:173–180.
7. Ptasznik R, Hennesy O. Abnormalities of the biceps tendon of the shoulder: sonographic findings. AJR Am J Roentgenol 1995; 164:409–414.
8. Prato N, Derchi LE, Martinoli C. Sonographic diagnosis of biceps tendon dislocation. Clin Radiol 1996; 51:737–739.
9. Farin PU. Sonography of the biceps tendon of the shoulder: normal and pathologic findings. J Clin Ultrasound 1996; 24:309–316.
10. Farin PU, Jaroma H, Harju A, Soimakallio S. Medial displacement of the biceps brachii tendon: evaluation with dynamic sonography during maximal external shoulder rotation. Radiology 1995; 195:845–848.
11. Farin PU, Jaroma H. The bicipital groove of the humerus: sonographic and radiographic correlation. Skeletal Radiol 1996; 25:215–219.
12. Lee J, Brookenthal KR, Ramsey ML, Kneeland JB, Herzog R. MR imaging assessment of the pectoralis major myotendinous unit: an MR imaging-anatomic correlative study with surgical correlation. AJR Am J Roentgenol 2000; 174:1371–1375.
13. Bianchi S, Zwass A, Abdelwahab I. Sonographic evaluation of posterior instability and dislocation of the shoulder. J Ultrasound Med 1994; 13:389–393.
14. Schydlowsky P, Strandberg C, Galatius A, Gam A. Ultrasonographic examination of the glenoid labrum of healthy volunteers. Eur J Ultrasound 1998; 8:85–89.
15. Hammar MV, Wintzell GB, Astom KGO, Larsson S, Elvin A. Role of US in the preoperative evaluation of patients with anterior shoulder instability. Radiology 2001; 219:29–34.
16. Schydlowsky P, Strandberg C, Galbo H, Krogsgaard M, Jorgensen U. The value of ultrasonography in the diagnosis of labral lesions in patients with anterior shoulder dislocation. Eur J Ultrasound 1998; 8:107–113.
17. Taljanovic MS, Carlson KL, Kuhn JE, Jacobson JA, Delaney-Sathy LO, Adler RS. Sonography of the glenoid labrum: a cadaveric study with arthroscopy correlation. AJR Am J Roentgenol 2000; 174:1717–1722.
18. Farin PU, Kaukanen E, Jaroma H, Harju A, Vaatainen U. Hill-Sachs lesion: sonographic detection. Skeletal Radiol 1996; 25:559–562.

19. Pancione L, Gatti G, Mecozzi B. Diagnosis of Hill-Sachs lesion of the shoulder. Acta Radiol 1997; 38:523–526.
20. Cicak N, Bilic R, Delimar D. Hill-Sachs lesion in recurrent shoulder dislocation: sonographic detection. J Ultrasound Med 1998; 17:557–560.
21. Patten RM, Mack LA, Wang KY, Lingel J. Nondisplaced fractures of the greater tuberosity of the humerus: sonographic detection. Radiology 1992; 182:201–204.
22. Tossy JD, Mead NC, Sigmond HM. Acromioclavicular separations: useful and practical classification for treatment. Clin Orthop 1963; 28:111–119.
23. Kock HJ, Jurgens C, Hirche H, Hancke J, Schmit-Neuerburg KP. Standardized ultrasound examination for evaluation of instability of the acromioclavicular joint. Arch Orthop Trauma Surg 1996; 115:136–140.
24. Yu YS, Dardani M, Fisher RA. MR observations of posttraumatic osteolysis of the distal clavicle after traumatic separation of the acromioclavicular joint. J Comput Assist Tomogr 2000; 24:159–164.
25. Grainger AJ, Tirman PFJ, Elliott JM, Kingzett-Taylor A, Steinbach LS, Genant HK. MR anatomy of the subcoracoid bursa and the association of subcoracoid effusion with tears of the anterior rotator cuff and the rotator interval. AJR Am J Roentgenol 2000; 174:1377–1380.
26. Ptasznik R. Sonography of the shoulder. In: van Holsbeeck MT, Introcaso JH, eds. Musculoskeletal ultrasound. Philadelphia, Pa: Saunders, 1997; 463–516.
27. Bureau NJ, Dussault RG, Keats TE. Imaging of bursae around the shoulder joint. Skeletal Radiol 1996; 25:513–517.
28. van Holsbeeck M, Strouse PJ. Sonography of the shoulder: evaluation of the subacromial-subdeltoid bursa. AJR Am J Roentgenol 1993; 160:561–564.
29. Alasaarela EM, Alasaarela EL. Ultrasound evaluation of painful rheumatoid shoulders. J Rheumatol 1994; 21:1642–1648.
30. Gibbon WW, Wakefield RJ. Ultrasound in inflammatory disease. Radiol Clin North Am 1999; 37: 633–651.
31. Alasaarela E, Leppilahti J, Hakala M. Ultrasound and operative evaluation of arthritic shoulder joints. Ann Rheum Dis 1998; 57:357–360.
32. Lange U, Teichmann J, Stracke H, Bretzel RG, Neeck G. Elderly onset rheumatoid arthritis and polymyalgia rheumatica: ultrasonographic study of the glenohumeral joints. Rheumatol Int 1998; 17: 229–232.
33. Koski JM. Ultrasonographic evidence of synovitis in axial joints in patients with polymyalgia rheumatica. Br J Rheumatol 1992; 31:201–203.
34. Cantini F, Salvarani C, Olivieri I, et al. Shoulder ultrasonography in the diagnosis of polymyalgia rheumatica: a case-control study. J Rheumatol 2001; 28:1049–1055.
35. Bianchi S, Martinoli C. Detection of loose bodies in joints. Radiol Clin North Am 1999; 37:679–690.
36. Peetrons P, Rasmussen OS, Creteur V, Chhem RK. Ultrasound of the shoulder joint: non "rotator cuff" lesions. Eur J Ultrasound 2001; 14:11–19.
37. Kay J, Benson CB, Lester S, et al. Utility of high-resolution ultrasound for the diagnosis of dialysis-related amyloidosis. Arthritis Rheum 1992; 35: 926–932.
38. Cardinal E, Buckwalter KA, Braunstein EM, Raymond-Tremblay D, Benson MD. Amyloidosis of the shoulder in patients on chronic hemodialysis: sonographic findings. AJR Am J Roentgenol 1996; 166:153–156.
39. Sommer R, Valen GJ, Ori Y, et al. Sonographic features of dialysis-related amyloidosis of the shoulder. J Ultrasound Med 2000; 19:765–770.
40. Cardinal E, Bureau NJ, Aubin B, Chhem RK. Role of ultrasound in musculoskeletal infections. Radiol Clin North Am 2001; 39:191–201.
41. Lombardi T, Sherman L, van Holsbeeck M. Sonographic detection of septic subdeltoid bursitis: a case report. J Ultrasound Med 1992; 11: 159–160.
42. Widman DS, Craig JG, van Holsbeeck MT. Sonographic detection, evaluation and aspiration of infected acromioclavicular joints. Skeletal Radiol 2001; 30:388–392.
43. Fehrman DA, Orwin JF, Jennings RM. Suprascapular nerve entrapment by ganglion cysts: a report of six cases with arthroscopic findings and review of literature. Arthroscopy 1995; 11:727–734.
44. Hashimoto BE, Hayes AS, Ager JD. Sonographic diagnosis and treatment of ganglion cysts causing suprascapular nerve entrapment. J Ultrasound Med 1994; 13:671–674.
45. Chiou HJ, Chou YH, Wu JJ, et al. Alternative and effective treatment of shoulder ganglion cyst: ultrasonographically guided aspiration. J Ultrasound Med 1999; 18:531–535.
46. Linker CS, Helms CA, Fritz RC. Quadrilateral space syndrome: findings at MR imaging. Radiology 1993; 188:675–676.
47. Loomer R, Graham B. Anatomy of the axillary nerve and its relation to inferior capsular shift. Clin Orthop Rel Res 1989; 243:100–105.
48. Sanders TG, Tirman PFJ. Paralabral cyst: an unusual cause of quadrilateral space syndrome. Arthroscopy 1999; 15:632–637.
49. Kransdorf MJ, Meis JM, Montgomery E. Elastofibroma: MR and CT appearance with radiologic-pathologic correlation. AJR Am J Roentgenol 1992; 159:575–579.
50. Bianchi S, Martinoli C, Abdelwahab IF, Gandolfo N, Derchi LE, Damiani S. Elastofibroma dorsi: sonographic findings. AJR Am J Roentgenol 1997; 169:1113–1115.

This article meets the criteria for 1.0 credit hour in category 1 of the AMA Physician's Recognition Award. To obtain credit, see accompanying test at http://www.rsna.org/education/rg_cme.html.